Effect of Specimen History on Structure and In-Plane Permeability of Woven Fabrics

A. Endruweit*, X. Zeng and A.C. Long
Faculty of Engineering – Division of Materials, Mechanics & Structures,
University of Nottingham, University Park, Nottingham, NG7 2RD, U.K.
* Corresponding author (Email: andreas.endruweit@nottingham.ac.uk)

Abstract

Before being processed into composites, reinforcement fabrics may undergo repeated involuntary deformation, the complete sequence of which is here referred to as specimen history. To mimic its effect, fabric specimens were subjected to sequences of defined shear operations. For single fabric layers with unconstrained thickness, quantitative evaluation of photographic image data indicated that repeated shear deformation results in a residual increase in inter-yarn gap width. This translates into an increase in measured fabric permeabilities in multi-layer lay-ups at given compaction levels. The extent of both interrelated effects increases with increasing yarn density in the fabric and with increasing maximum angle in the shear history. Additional numerical permeability predictions indicated that the increase in permeability may be partially reversed by through-thickness fabric compression. The observations suggest that the effect of involuntary deformation of the fabric structure can result in variations in the principal permeability values by factors of up to 2.

Keywords

Liquid Composite Moulding, textile fabric, permeability, reproducibility, shear

Introduction

In Liquid Composites Moulding (LCM) processes, the impregnation of textile reinforcements with liquid resin systems is frequently described by the model of a viscous liquid flowing through a porous medium, characterised by its porosity and permeability. Determination of the textile permeability is a prerequisite for optimisation of the process parameters for production of composite components applying LCM-technology, in particular location of injection gates and vents in the mould to achieve complete impregnation of the reinforcement, and for prediction of the mould fill time.

Experimentally observed permeability values frequently show large scatter. As an example, a recent international benchmark exercise, [1] which gave an overview of methods for permeability measurement in practical use in different laboratories and the range of results obtained implementing these methods, indicated that in-plane permeability values for a given woven reinforcement fabric, measured in different laboratories, can show a scatter of one order of magnitude at any given fibre volume fraction (Figure 1). The ratio of the principal permeability values can vary by factors of up to 2. This variability makes resin flow during reinforcement impregnation hard to predict, and uncontrollable flow may eventually affect the composite manufacturing process and result in formation of defects in the component.

It was suspected that potential error sources causing scatter are related to measurement set-up and execution of experiments. This was confirmed when a follow-up study,[2] where measurement methods and procedures were standardised, showed an apparent reduction in scatter. While the tested fabric specimens had identical nominal properties, an additional source of the observed variability may be related to the different history of different material batches and its influence on the actual fabric structure. It can be speculated that variations in the structure of tested fabrics may be operator-induced during specimen preparation (fabric

cutting, stacking of multi-layer specimens) or result from effects of gravity and handling during storage and transport.

Since shear, the mechanics of which was discussed in detail by Behre[3] and Skelton,[4] is the main deformation mechanism of woven fabrics,[5] the specimen history can be assumed to affect the fabric structure mainly through involuntary (repeated) shear. The residual effect of the specimen shear history on the fabric structure (illustrated schematically in Figure 2, and sometimes referred to as "mechanical fabric conditioning"), i.e. the difference in structure between the initial 0°/90° configuration and the final configuration restored to 0°/90°, is related to the forces which need to be applied to overcome constraints on yarn rotation in order to shear a fabric. In densely packed fabrics, constraints on the yarn mobility result mainly from contact forces between parallel yarns (Figure 3(a)). In coarse woven fabrics, constraints on yarn rotation are imposed by crimp (interaction of initially orthogonal yarns) as discussed by Nguyen et al.[6] and friction in cross-over points (Figure 3(b)). In the former case, forces tend to be significantly higher than in the latter case. In either case, forces applied to shear a fabric translate into lateral yarn compression, potentially resulting in a residual reduction in yarn width and a residual increase in inter-yarn gap width.

While the permeability of woven fabrics sheared to given fibre angles was studied before, e.g. by Hammami et al.,[7] Smith et al.,[8] Lai and Young[9] and Bickerton et al.,[10] this study aims at characterising the residual effect of the specimen history, mimicked by repeatedly shearing a fabric to given angles in given directions, on the fabric structure. It also aims at describing how the potential change in inter-yarn gap width in a single fabric layer with unconstrained thickness transfers into a change in permeability in a multi-layer lay-up at given levels of through-thickness compaction.

Fabric geometry analysis

Materials

The effect of repeated shear on the fabric structure was studied for two 2×2 twill weave carbon fibre fabrics, one with nominal superficial density S_0 = 660 g/m^2 and filament count c_f = 12K, the other with S_0 = 285 g/m^2 and c_f = 6K. The photographs in Figure 4 indicate the difference in yarn packing density in both (unsheared) fabrics.

Method

To simulate the effect of the material history for different woven fabrics, single-layer fabric specimens with unconstrained thickness were sheared to given angles and subsequently restored to a 0/°90° configuration. A steel shear frame (Figure 5(a)) was used, where rectangular specimens with dimensions 500 mm × 280 mm were clamped along the short edges which were parallel to either the fabric warp or weft direction. Analysis of photographs of the fabric surface, acquired after completion of each shear cycle (i.e. restored to a 0/°90° configuration) using a flatbed document scanner, allowed yarn spacing, s_y, and yarn width, w_y, to be measured in 2D projection. The width of inter-yarn gaps, w_g, can then be identified as the difference of s_y and w_y. Potential changes in yarn thickness related to changes in yarn width were not quantified here.

Starting from the initial unsheared configuration, the shear angle was increased in steps of 5°. The specimens were sheared alternately in both possible directions, indicated as "+" and "-". For example, a specimen characterised by a shear history with a maximum shear angle of +10° would have undergone shear to the following angles: 0+ ,°5 ,°0- ,°5 ,°0+ ,°10 ,°0°. This sequence corresponds to three shear cycles, since one cycle is considered completed every time the fabric is sheared to a given angle and back to 0°.

Results

For specimens of the two 2×2 twill weave carbon fibre fabrics described above, yarn widths, w_y, measured for unsheared specimens and specimens after undergoing shear to a maximum angel of -40° are listed in Table 1. Each value is based on 20 measurements from a sampling area of approximately 100 mm × 100 mm (as indicated in Figure 5(a)). The data acquired here do not enable any statistical distribution of the yarn widths to be clearly identified. Average inter-yarn gap widths, w_g, after undergoing different shear operations are plotted in Figures 6 and 7. The absolute value of the maximum shear angle was limited to 40° since considerable force needs to be applied to shear the fabric any further (as will be discussed below). This is considered prohibitive for involuntary deformation, which these experiments attempt to mimic.

For interpretation of the results, several caveats are to be considered. Although, for each fabric, all specimens are from the same batch (same roll) of material, every "unsheared" specimen has undergone its own specific history (cutting, transfer into the shear frame, clamping) before the experiment, which may result in different initial configurations. The effect of induced shear on the fabric structure may vary depending on the accuracy of alignment of the fabric specimens in the shear frame, which may be limited by the manual process, and there may be some slack the in fabric affecting tension in the yarns when sheared. In addition, the accuracy of shear angle adjustment is limited. Finally, evaluation of images of the specimen surface may introduce uncertainty. Blurred images explain the outliers in Figure 7.

Despite these known issues, the following trends can be derived from the acquired data. Figure 6 indicates that, prior to any shear operation, no gaps exist between parallel fibre bundles in the fabric with S_0 = 660 g/m^2, and there is no significant difference in widths of warp and weft yarns (Table 1). After undergoing shear operations, there are only small

changes in yarn width for small maximum angles in the shear history (shear cycles 1 to 7). For maximum angles in the shear history greater than approximately 20° (shear cycles 7 to 16), which coincides with the observed onset of wrinkling in the fabric, the increase in gap width, i.e. decrease in yarn width, becomes stronger. This trend is stronger when the fabric is clamped along the warp direction than when clamped along the weft direction. In this case, the weft yarns seem to get slightly wider at small maximum angles resulting in partial overlap of adjacent bundles, which translates into a negative gap width (the yarn width is measured at approximately the widest point of the yarns). The difference between the initial and final yarn width (maximum shear angle -40°) is approximately identical in both fabric directions.

In the fabric with S_0 = 285 g/m^2 (Figure 7), gaps exist between parallel fibre bundles prior to any shear operation. These initial gaps are significantly wider between weft yarns than between warp yarns, which is related to a significant difference in yarn width (warp yarns are wider than weft yarns) as indicated in Table 1. After undergoing shear operations, the gap widths increase approximately linearly with increasing maximum angle in shear history (i.e. the yarn widths decrease). The increase in gap width is more significant between warp yarns than between weft yarns, i.e. the reduction in yarn width is stronger for warp yarns, which are initially wider than weft yarns. There appears also to be a trend for the gap widths to increase more strongly when the fabric is clamped along the weft direction than when clamped along the warp direction, which may be related to different yarn mobility in the different fabric directions. Since this trend is weak, it will be ignored in the following. For this fabric, no wrinkling was observed in the range of shear angles discussed here.

It was expected that lateral forces onto yarns, repeatedly applied during the specimen shear history, would result in straightening of yarns and that, as a result, the variability in local yarn width and inter-yarn gap width would reduce with increasing number of shear operations. However, this effect could not be verified based on the observed data, which do

not suggest any dependence of the standard deviations of the yarn width on the specimen shear history (Table 1).

Shear resistance measurement

Method

Fabric shear resistance data were measured to help understand the fabric mechanics leading to the observed changes in the fabric structure. Picture frame shear tests[5] were carried out on an Instron 5969 testing machine with a 5 kN load cell. The cross-head speed was set to 20 mm/min. Deviating from the normal procedure for picture frame shear tests (where cross-shaped specimens are used), rectangular fabric specimens were clamped along the short edges (Figure 5(b)), parallel either to the fabric warp or weft direction, to be consistent with the procedure employed for fabric geometry analysis. Here, the dimensions of the specimens were 200 mm × 100 mm. The difference in specimen area compared to the specimens for geometry analysis affects the absolute values of shear resistance, but not the qualitative fabric behaviour at different shear angles.

The cross-head displacement, d, on the testing machine (Figure 8) was converted to fabric shear angles, γ, according to

$$\gamma = \frac{\pi}{2} - 2\theta \quad , \tag{1}$$

where

$$\theta = \arccos\left(\frac{d}{2L} + \frac{1}{\sqrt{2}}\right) \tag{2}$$

is half the angle between fibre directions in the fabric,[5] and L is the side length of the shear frame. This allowed the same shear cycles as for geometry analysis to be reproduced.

Results

For the fabrics described above and shown in Figure 4, the shear angle was calculated according to Eq. (1). As suggested by Cao et al.,[5] the shear force, F_s, was calculated from the force applied to the picture frame, F_t, corrected by the force required to shear the empty frame, F_f, according to

$$F_s = \frac{F_t - F_f}{2\cos\theta} \quad . \tag{3}$$

Typical results for all shear cycles are plotted in Figures 9(a) and 10(a) (for clarity, only the loading phase of each shear cycle is plotted, the unloading phase is omitted). For evaluation of the data, the same caveats as for geometry analysis apply. Of particular concern is the accuracy of specimen alignment in the picture frame. Even slight misalignment may result in asymmetry of the curves (as in Figure 9(a), for S_0 = 660 g/m^2) due to an offset in shear angle and tension induced in the fibres.

For the fabric with S_0 = 660 g/m^2, detailed analysis of the data plotted in Figures 9(b) and 9(c) suggest that, for shear cycles with maximum shear angles of up to approximately 20° (cycles 1 to 7), the shear force as a function of the shear angle follows approximately the same trace in each cycle. If the maximum angle is greater than approximately 20° (cycles 7 to 16), the absolute value of the shear force in each cycle is smaller than in previous cycles (in the range of shear angles smaller than the maximum angles in previous cycles). Increasingly more additional force is required in the range of shear angles greater than the maximum angles in previous cycles.

For the fabric with S_0 = 285 g/m^2, absolute values of force applied to shear the fabric to a given angle are smaller than for the other fabric. In each cycle, the shear force is smaller than in previous cycles (Figure 10(b)). The difference appears to increase approximately linearly with increasing maximum shear angle (Figure 11). The additional force required in the range

of shear angles greater than the maximum angles in previous cycles appears to drop off with increasing maximum angle.

In-plane permeability measurement

Method

For the 2×2 twill weave carbon fibre fabric with S_0 = 660 g/m^2, the in-plane permeability was characterised experimentally in unsaturated flow experiments with radial injection geometry at constant injection pressure. Synthetic oil with known viscosity-temperature characteristics (103 mPa×s at 20 °C) was used as a test fluid.

At a cavity height of 2 mm, specimens consisted of 3 fabric layers, corresponding to a fibre volume fraction V_f = 0.56. All layers had the same orientation. Specimens were prepared by shearing each fabric layer individually before stacking, following the procedure described above. Shear angles were increased in steps of 5° (alternating in "+" and "-" direction) until the target maximum angle was reached. Areas which may have been damaged by clamping of the fabric in the shear frame were cut from the originally rectangular layers prior to injection. The resulting square specimens with dimensions 280 mm × 280 mm were used for the injection experiments.

For the fabric with S_0 = 285 g/m^2, the permeability was measured in a previous series of unsaturated injection experiments with linear injection geometry at constant injection pressure.[12] At a cavity height of 3.5 mm, 9 fabric layers corresponded to V_f = 0.40. Experimental permeability data are available only for unsheared specimens.

Results

For the fabric with S_0 = 660 g/m^2, results for the measured in-plane permeability of specimens with different history are listed in Table 2 (3 repeats each; constant injection

pressure in range from 1.68 bar to 1.83 bar). For both clamping configurations, the principal in-plane permeability values, K_1 and K_2, increase approximately linearly with increasing maximum shear angle (Figure 12). The increase tends to be slightly stronger for specimens clamped along the warp direction than for those clamped along the weft direction. There is no clear trend for the ratio K_1/K_2 to change. The ratio of the semi-major and semi-minor axes of the flow front ellipse in radial flow, R_1/R_2, which is equal to the square root of the ratio K_1/K_2, is approximately constant at a value of 1.2. This implies that the flow front shape is similar to a circle, and the principal flow direction is sensitive to small changes in fabric structure. This is reflected in the observed changes in the angle β, which indicates the orientation of K_1 relative to the fabric weft direction.

For the fabric with S_0 = 285 g/m^2, the measured permeability is given in Table 3 (10 repeats at 0 ,°45° and 90° between warp direction and applied pressure gradient; constant injection pressure in range from 0.80 bar to 1.22 bar). Here, the principal flow direction coincides with the weft direction, because the gap width between weft yarns tends to be significantly higher than the gap width between warp yarns (Figure 7).

In-plane resin flow simulation

Method

To complement experimental data, permeabilities were predicted based on resin flow simulations. This allows identifying clearly the correlation between geometrical fabric parameters, which can be controlled for the simulations, and permeabilities. Based on the data in Table 1, Figure 6, and additional 3D geometry data (Figure 13) for unsheared specimens acquired using micro-Computed Tomography (μ-CT), geometrical models of 3 layers of the fabric with S_0 = 660 g/m^2 at a cavity height of 2 mm (corresponding to the experiments for permeability measurement) were generated using the software TexGen.[13]

The dimensions of the models were chosen such that one complete fabric unit cell (4 × 4 yarns) was included in each layer. For relative positioning of the layers, two cases, zero nesting and random nesting, were considered. To model random nesting, the relative in-plane displacement of layers was normalised over the full length of one unit cell in weft- and warp-direction. Instances of random nesting were generated employing Latin hypercube sampling[14] from randomly distributed displacement values. Compared to Monte Carlo sampling, this produces more evenly distributed samples from the entire ranges of variables, thus allowing to fully explore multi-dimensional inputs based on limited numbers of simulations. Modelling of each individual ply was based on geometrical continuity and imposed geometrical constraints. Issues of stochastic variability in yarn paths and yarn cross-sections in each ply, which were discussed by Vanaerschot et al.,[15] were not considered here.

In a first step, the geometrical model of the unsheared fabric was generated in an automatic manner based on the measured geometrical data in Table 1. The principles of geometrical fabric modelling are discussed in detail by Lin et al.[16] To avoid yarn intersections at cross-over points, realistic yarn paths were defined automatically accounting for fabric crimp, and yarn cross-sectional geometries were adapted locally by changing widths and heights. Then, observed changes in yarn widths due to the fabric shear history (Figures 6 and 7) were introduced successively through manual updates of the respective yarn widths in the model geometries. The simplifying assumption was made that the yarn width in a lay-up at given level of compaction is the same as the width in a single fabric layer with unconstrained thickness, i.e. potential flattening and widening of the yarns due to through-thickness compression was ignored here (Figure 14). The implications of this assumption will be discussed below.

The geometrical models were used to generate flow domains for Computational Fluid Dynamics (CFD) simulations containing yarns and the surrounding empty spaces in the tool

cavity. The flow domains were meshed with uniform hexahedral (brick shaped) voxels with appropriate size for representation of a sufficient level of geometrical detail. The permeabilities of yarns, which can be estimated based on the models proposed by Gebart[17] assuming ideal square or hexagonal filament arrangement, are typically small compared to the overall permeabilities of the fabric stacks. Thus, the yarns can be assumed to be impermeable in order to reduce the computational cost for CFD simulations. Steady-state Navier-Stokes flow through the pore spaces was simulated using the commercial CFD code Ansys CFX™. The assumptions of yarn impermeability and steady state (i.e. saturated) flow imply that capillary effects, which may affect the unsaturated flow experiments for permeability measurement described above, are not considered in the simulations. Translational periodic boundary conditions were set on opposite faces of the textile unit cell domain in weft and warp direction to represent a continuous reinforcement. A flow-driving pressure drop was applied in either warp or weft direction. No-slip wall boundary conditions were specified at the top and bottom faces of the domain to simulate flow along the mould surfaces during in-plane fabric impregnation. Since inter-yarn gap spaces are typically large compared to pore spaces in the yarns, implying that lubrication at the yarn-gap interface can be assumed to be negligible,[18] no-slip boundary conditions were also applied on the yarn surfaces. From the applied pressure gradients along different fabric directions and the calculated average flow velocities, in-plane permeabilities were determined. In a first step, the mesh sensitivity of the predicted permeabilities was assessed. Based on the results of simulations with different mesh densities, the number of voxels for the entire flow domain was chosen as 150 × 150 × 90 (warp × weft × thickness) to obtain a reasonable balance between computation time and accuracy for all following simulations.

The same procedure was applied to modelling flow through 9 layers of the fabric with S_0 = 285 g/m^2 at a cavity height of 3.5 mm. A mesh with 150 × 150 × 270 hexahedral voxels was

used for the flow simulations, for which convergence of the results was found. As for the other fabric, cases with zero nesting and random nesting were simulated.

Results

Examples for geometrical models of unsheared fabric (S_0 = 660 g/m^2) with zero nesting and random nesting are shown in Figure 15. In the models, weft yarns are oriented along the *x*-direction, warp yarns are oriented along the *y*-direction.

Results for the permeabilities in both fabric directions, derived from the results of CFD simulations, are listed in Table 4. In the case of random nesting, six example lay-ups were generated for each shear history, and average permeabilities and standard deviations were determined. The data indicate that, in addition to the effect of nesting, which was discussed by Hoes et al.,[19] the fabric history has a significant effect on the permeability. Computed permeabilities are higher for random nesting than for zero nesting, reflecting different geometries of flow channels forming in the lay-up. The permeability in the weft direction, K_x, is consistently higher than the permeability in the warp direction, K_y. The ratio K_x/K_y tends to be higher for zero nesting than for random nesting. With increasing maximum angle in the shear history, K_x and K_y increase since the inter-yarn gap width increases as illustrated in Figure 6.

For the fabric with S_0 = 285 g/m^2, permeabilities in both fabric directions, derived from the CFD simulations, are listed in Table 5 (six example lay-ups for random nesting). Due to lack of experimental data for comparison, only results for the unsheared fabric and a shear history with a maximum shear angle of -40° are listed here. After undergoing the shear operations, the permeability in both fabric directions is higher than for the unsheared fabric, since the inter-yarn gap widths increase as illustrated in Figure 7. The permeability in the weft direction is consistently higher than the permeability in the warp direction. The ratio of

permeability values in the different fabric directions tends to be higher for zero nesting than for random nesting. It is smaller for the fabric that has undergone the shear operations than for the unsheared fabric.

Discussion

For the fabric with S_0 = 660 g/m^2, parallel yarns are in contact with each other if previously unsheared (Figure 4), suggesting that contact forces between parallel yarns (Figure 3(a)) are the main deformation mechanism in fabric shear. The average yarn width in the fabric decreases with increasing maximum angle in the shear history, and the gap width increases accordingly. The residual effect of shear on the gap width is small for small maximum shear angles, but more significant for shear angles greater than the angle for onset of fabric wrinkling at approximately 20° (Figure 6).

These geometrical observations correlate well with the measured shear resistance data (Figure 9), which suggest that lateral yarn compression is almost "elastic" for shear angles up to approximately 20° and relatively small shear forces. For greater shear angles, where wrinkling was observed, the force in each shear cycle is reduced compared to the previous one (in the range of angles reached in previous cycles). This suggests that, in each cycle, the fabric loses part of its shear resistance due to "plastic" yarn deformation. The related creation and widening of inter-yarn gaps implies that the effect illustrated in Figure 3(b) is dominant for a range of shear angles, γ, with $\cos\gamma \times w_g > 0$ (where w_g is the gap width at the start of the cycle). With increasing shear angle (beyond angles reached in previous cycles), increasingly more force is required due to stiffening of the yarns in lateral compression with increasing density of filament packing (and increasing yarn thickness) at reduced yarn width.

For the fabric with S_0 = 285 g/m^2, geometrical considerations, based on values for w_y and s_y, indicate that, independent of the clamping configuration, adjacent weft yarns are in contact

only if the shear angle is greater than approximately 34°, adjacent warp yarns are in contact if the shear angle is greater than approximately 25°. While there are no contact forces between parallel yarns in any direction for shear angles smaller than 25°, the observed approximately linear reduction in yarn width with increasing maximum shear angle (Figure 7) is related to friction in yarn cross-over points and constraints on rotational yarn movement imposed by crimp (Figure 3(b)). The difference in the main mechanism for lateral yarn compression implies that shear forces for the fabric with S_0 = 660 g/m^2 are greater than those for the fabric with S_0 = 285 g/m^2.

The linear reduction in yarn width correlates with the measured shear resistance data (Figure 10), which indicate that the absolute value of the shear force in each cycle is smaller than in previous cycles. This suggests that, in each shear cycle, the fabric loses part of its shear resistance due to "plastic" yarn deformation. The additional force required for fabric shear in the range of angles greater than the maximum angles in previous shear cycles appears to drop off with increasing maximum angle, suggesting that, in the range of angles discussed here, reduction of the yarn width is not sufficient to result in stiffening in lateral compression.

This difference in behaviour compared to the fabric with S_0 = 660 g/m^2 is related to the yarn cross-sectional shape and filament count. As illustrated in Figure 4 and Table 1, yarn widths in both fabrics are similar. However, in the fabric with higher S_0 and c_f = 12K, the yarns have greater thickness due to constraints on the maximum yarn width. This lateral pre-compression is thought to result in higher resistance to permanent filament reordering in the yarns. On the other hand, in the fabric with lower S_0 and c_f = 6K, yarns are flatter and, due to lack of constraints on the cross-sectional dimensions, are thought to be more susceptible to filament reordering. Hence, the yarns deform more easily in fabric shear.

For the fabric with S_0 = 660 g/m^2, a shear history with a maximum angle of -40° resulted in a reduction in yarn width by 9 % or 10 % (Table 1) and the corresponding creation of inter-yarn gaps. For the same shear history, an increase in permeabilities by a factor of approximately 1.8 (clamped along warp) or 1.7 (clamped along weft) was observed experimentally. This indicates a correlation between changes in the fabric structure and measured permeability values at different shear histories.

Measured (Table 2) and predicted (Table 4) permeability values for specimens sheared while clamped along the fabric weft direction are compared in Figure 16, where K_x is assumed to correspond to K_1, K_y to K_2. This ignores changes in the orientation of the principal flow directions, which is sensitive to small changes in the fabric structure since the fabric properties are similar in both fabric directions. For the unsheared fabric and the fabric with a shear history with a maximum angle of -20°, predicted permeability values are similar to measured values. This implies that the assumptions made in numerical modelling (impermeability of yarns, negligible capillary effects) are valid. A further increase in the maximum angle in shear history results in an increasing difference between measured and predicted permeabilities, where the predictions overestimate the experimental data by significant margins. This difference suggests that the reduction in yarn width (and potential increase in yarn thickness) caused by shear in single fabric layers with unconstrained thickness is partially reversed by yarn flattening and widening in through-thickness compression of multiple fabric layers when stacked in the cavity during fluid injection, which is not considered in the computational model (Figure 14). However, the increase in inter-yarn gap width induced in the uncompressed fabric layers is at least partially conserved. The accuracy of simulation-based permeability predictions for specimens with large maximum angles in the shear histories is expected to improve when the simplified geometrical yarn models in Figure 14 are updated with more accurate 3D data, which can be acquired

employing μ-CT to allow the effect of yarn flattening and widening for compressed stacks of fabric layers to be quantified. In particular, more accurate modelling of the increased actual width of flattened yarns is expected to result in a reduction in predicted permeability values for large shear angles.

For the fabric with S_0 = 285 g/m^2, the accuracy of permeability predictions based on flow simulations for the unsheared fabric improved significantly compared to previous simulations[12] (where prediction for K_{warp} were in the range between 3.00×10^{-10} m^2 and 3.24×10^{-10} m^2, and for K_{weft} between 3.33×10^{-10} m^2 and 3.43×10^{-10} m^2), because more accurate geometry data were available. A shear history with a maximum angle of -40° resulted in an observed increase in inter-yarn gap width in the order of 80 % (between warp yarns) and 30 % (between weft yarns), respectively. This significant increase in gap width in a single layer transferred into an increase in predicted permeability of a fabric lay-up. After undergoing the shear operations, the predicted permeability is less anisotropic than in the unsheared fabric, because the difference in gap widths in both fabric directions is reduced (Figure 7). However, the predicted change in permeability caused by the shear history is significantly smaller than for the fabric with S_0 = 660 g/m^2, because the relative change in inter-yarn gap widths is smaller (Figures 6 and 7). As for the other fabric, yarn flattening and widening in through-thickness compression is expected to reverse partially the increase in permeability caused by the fabric shear history.

To obtain additional information on the dependence of the residual effect on the fabric structure on the sequence of shear operations, two sets of additional experiments for geometry analysis were conducted. In the first set, specimens were sheared repeatedly to the same angle. Starting from 0°, the sequence +30 ,°0° was repeated five times. In the second set, the shear angle was reduced with increasing number of cycle. The shear sequence was 0 °, +40°, 0+ ,°30 ,°0+ ,°20°, 0+ ,°10°, 0°.

For the fabric with S_0 = 660 g/m^2, the measured inter-yarn gap width (Figure 17) shows a trend to keep increasing when the fabric is sheared repeatedly to the same angle (+30°). This implies that, after completion of the first cycle, there is still shear force translated into lateral yarn compression in the following cycles, although the applied force is significantly smaller than in the first cycle (Figure 9). When sheared repeatedly to angles which decrease with increasing number of shear operation, there appears to be no clear trend for the gap width in the fabric to change significantly after the first shear cycle.

For the fabric with S_0 = 285 g/m^2, results for the measured inter-yarn gap width (Figure 18) suggest that gaps between warp yarns are not affected when the fabric is sheared repeatedly to +30°. Gaps between weft yarns appear to decrease slightly in width, although this trend is very weak. This apparent small difference in behaviour in both fabric directions is related to the fabric structure. Since adjacent weft yarns are in contact only if the shear angle is greater than approximately 34°, it can be speculated that, due to relatively weak constraints on the yarn width, the relatively loose yarns can spread out when handled. This would explain a reduction in observed gap width. On the other hand, adjacent warp yarns are in contact if the shear angle is greater than approximately 25°, implying that the yarns are re-compressed laterally in each shear cycle. As a result, the yarn width (and gap width) does not change. No significant change in gap width was observed for repeated shear of the fabric to angles which decrease with increasing number of shear operation.

The issue of changes in through-thickness permeability was not addressed here. As does the in-plane permeability, the through-thickness permeability depends strongly on the width of inter-yarn gaps in each fabric layer. Hence, it is expected to exhibit a similar dependence on the fabric shear history as the in-plane permeability.

Conclusions

For two different 2×2 twill weave carbon fibre fabrics, the effect of specimen history on the fabric structure was mimicked by repeated defined shear deformation. For single fabric layers with unconstrained thickness, quantitative evaluation of photographic image data of the fabric surface in 0°/90° configuration indicated that repeated defined shear deformation results in a residual increase in inter-yarn gap width. Complimentary picture frame shear tests indicated different shear behaviour for both tested fabrics, which have different dominating deformation mechanisms. The densely packed fabric showed high shear resistance and a strong residual increase in inter-yarn gap width, while the coarse fabric showed low shear resistance and a weak increase in gap width. The increase in gap width translates into an increase in experimentally determined permeability values for multi-layer fabric stacks at given levels of through-thickness compaction. For the examples discussed here, an increase in permeability by up to 80 % was observed. Additional CFD analyses of resin flow were found to predict the experimental permeability data with reasonable accuracy provided that accurate geometry data are available. Comparison of predicted and measured permeability data for different fabric shear history implied that through-thickness compression of the fabric in the cavity partially reverses the increase in inter-yarn gap width induced in the uncompressed fabric layers.

It can be concluded that the effect of involuntary deformation of the fabric structure, e.g. during specimen handling, can result in variations in the principal permeability values by factors of up to 2.

Acknowledgement
This work was funded by the Engineering and Physical Sciences Research Council (grant number: EP/IO33513/1), through the EPSRC Centre for Innovative Manufacturing in Composites.

References

1. Arbter R, Beraud JM, Binetruy C, et al. Experimental Determination of the Permeability of Textiles: A Benchmark Exercise. *Compos Part A-Appl S* 2011; **42**(9): 1157-1168.

2. Vernet N, Ruiz E, Advani S, et al. Experimental determination of the permeability of engineering textiles: Benchmark II. *Compos Part A-Appl S* 2014; **61**: 172-184.
3. Behre B. Mechanical Properties of Textile Fabrics. Part I: Shearing. *Text Res J* 1961; **31**(2): 87-93.
4. Skelton J. Shear of Woven Fabrics. In: *Mechanics of Flexible Fibre Assemblies*, Sijthoff & Noordhoff, Alphen, 1980.
5. Cao J, Akkerman R, Boisse P, et al. Characterization of Mechanical Behavior of Woven Fabrics: Experimental Methods and Benchmark Results. *Compos Part A-Appl S* 2008; **39**(6): 1037–1053.
6. Nguyen M, Herszberg I and Paton R. The Shear Properties of Woven Carbon Fabric. *Compos Struct* 1999; **47**(1-4): 767-779.
7. Hammami A, Trochu F, Gauvin R, et al. Directional Permeability Measurement of Deformed Reinforcement. *J Reinf Plast Comp* 1996; **15**(6): 552-562.
8. Smith P, Rudd CD and Long AC. The Effect of Shear Deformation on the Processing and Mechanical Properties of Aligned Reinforcements. *Compos Sci Technol* 1997; **57**(3): 327-344.
9. Lai CL and Young WB. Model Resin Permeation of Fibre Reinforcements after Shear Deformation. *Polym Composite* 1997; **18**(5): 642-648.
10. Bickerton S, Simacek P, Guglielmi SE, et al. Investigation of Draping and Its Effect on the Mold Filling Process During Manufacturing of a Compound Curved Composite Part. *Compos Part A-Appl S* 1997; **28**(9-10): 801-816.
11. Wiggers J. Analysis of Textile Deformation during Preforming for Liquid Composite Moulding. PhD Dissertation, University of Nottingham, 2007.
12. Zeng XS, Long AC and Endruweit A. Numerical Prediction of Permeability of Textiles for the International Benchmark Exercise. In: *11th International Conference on Flow Processes in Composite Materials*, Auckland, 2012, pp. 2-9.
13. University of Nottingham. TexGen (Version 3.5.3), http://texgen.sourceforge.net (2012, accessed 26 March 2013).
14. McKay MD, Beckman RJ and Conover WJ. Comparison of Three Methods for Selecting Values of Input Variables in the Analysis of Output from a Computer Code. *Technometrics* 1979; **21**(2): 239–245.
15. Vanaerschot A, Cox BN, Lomov SV, et al. Stochastic framework for quantifying the geometrical variability of laminated textile composites using micro-computed tomography. *Compos Part A-Appl S* 2013; **44**: 122-131.
16. Lin H, Zeng X, Sherburn M, et al. Automated geometric modelling of textile structures. *Text Res J* 2012; **82**(16): 1689-1702.
17. Gebart BR. Permeability of Unidirectional Reinforcements for RTM. *J Compos Mater* 1992; **26**(8): 1100-1133.
18. Grouve WJB, Akkerman R. An idealised bc for the meso scale analysis of textile impregnation processes. In: *The 9th International Conference on Flow Processes in Composite Materials*, Montréal, 2008.
19. Hoes K, Dinescu D, Sol H, et al. Study of Nesting Induced Scatter of Permeability Values in Layered Reinforcement Fabric. *Compos Part A-Appl S* 2004; **35**(12): 1407-1418.

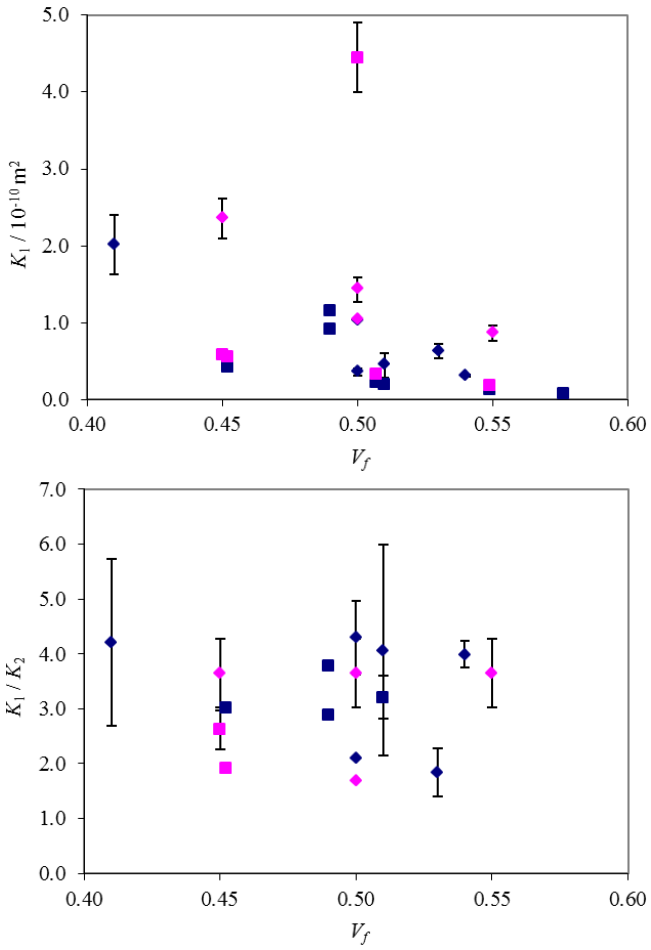

Figure 1. Scatter in permeability values measured by different laboratories for the example of a 2×2 twill weave glass fibre fabric:[1] principal permeability value, K_1, and ratio, K_1/K_2, as a function of fibre volume fraction, V_f; error bars indicate standard deviations.

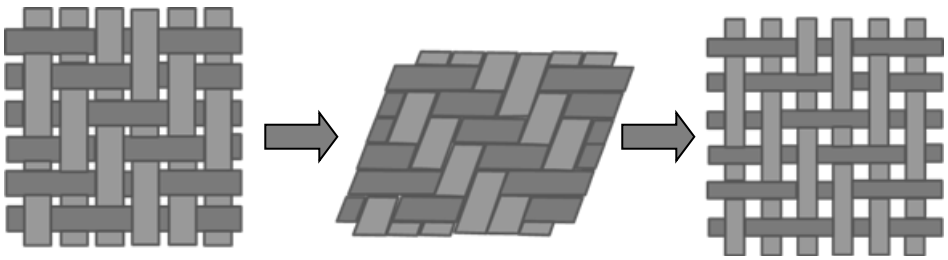

Figure 2. Residual effect of specimen shear history on fabric structure.

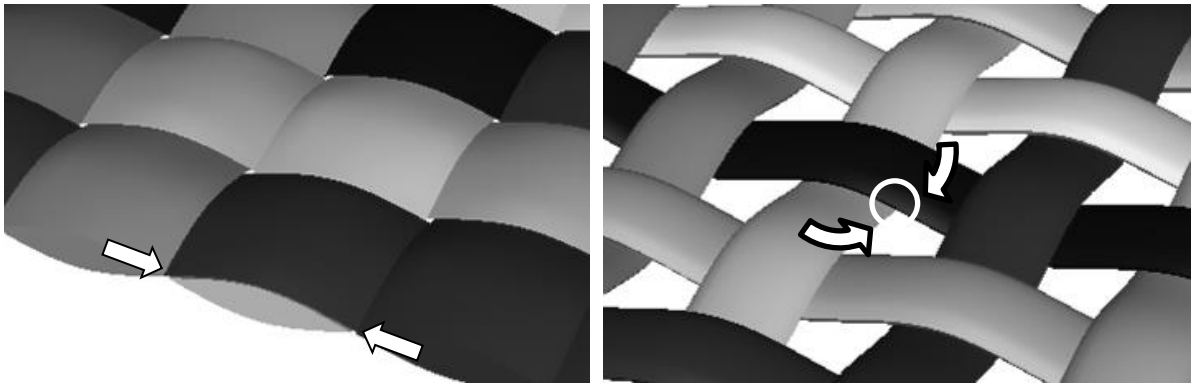

Figure 3. Mechanisms of lateral yarn compression; (a): contact forces between parallel yarns; (b): constraints on yarn rotation are imposed by crimp and friction at cross-over points; here: example plain weave.

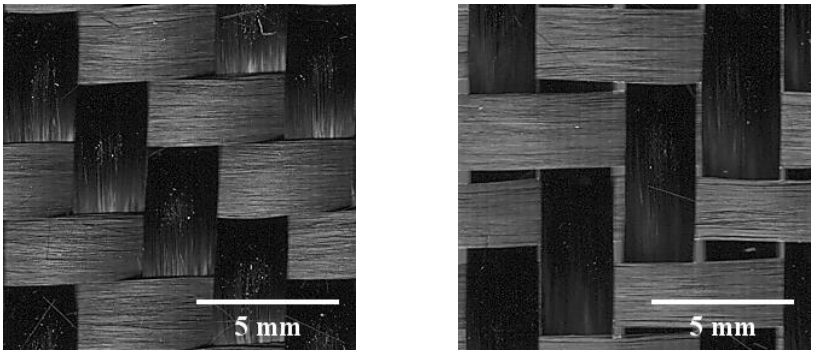

Figure 4. Surfaces of two different 2×2 twill weave fabrics, both unsheared; left: superficial density S_0 = 660 g/m^2, yarn filament count c_f = 12K; right: S_0 = 285 g/m^2, c_f = 6K.

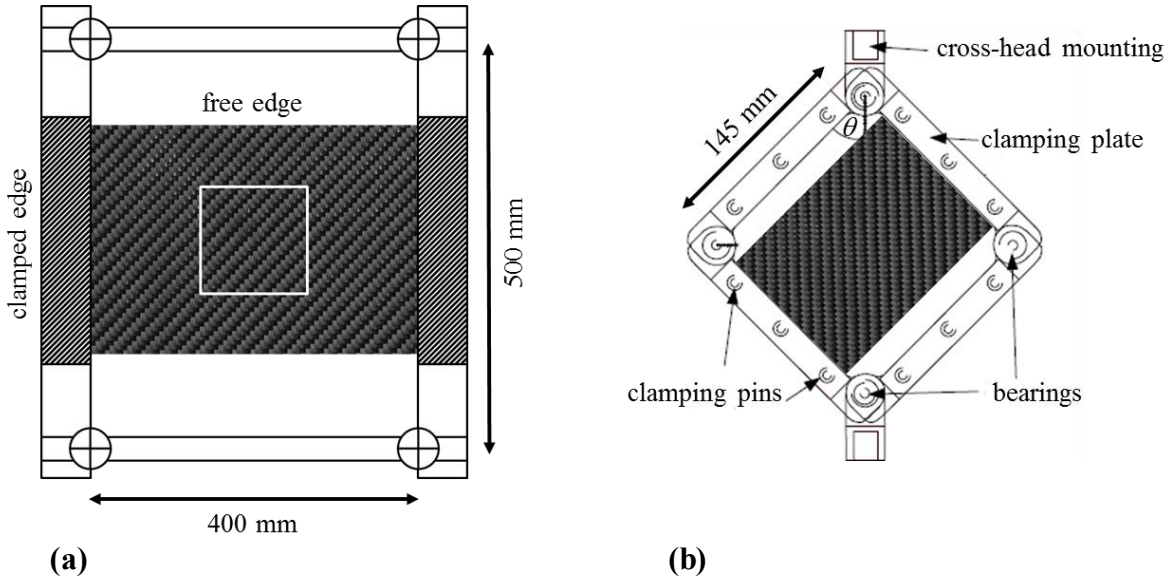

Figure 5. Schematic illustration of set-ups for fabric shearing; (a): steel frame allowing measurement of yarn spacing and yarn width in the fabric after undergoing defined shear deformations, white rectangle in centre indicates sampling area; (b): picture frame for shear resistance measurement (adapted from Wiggers[11]).

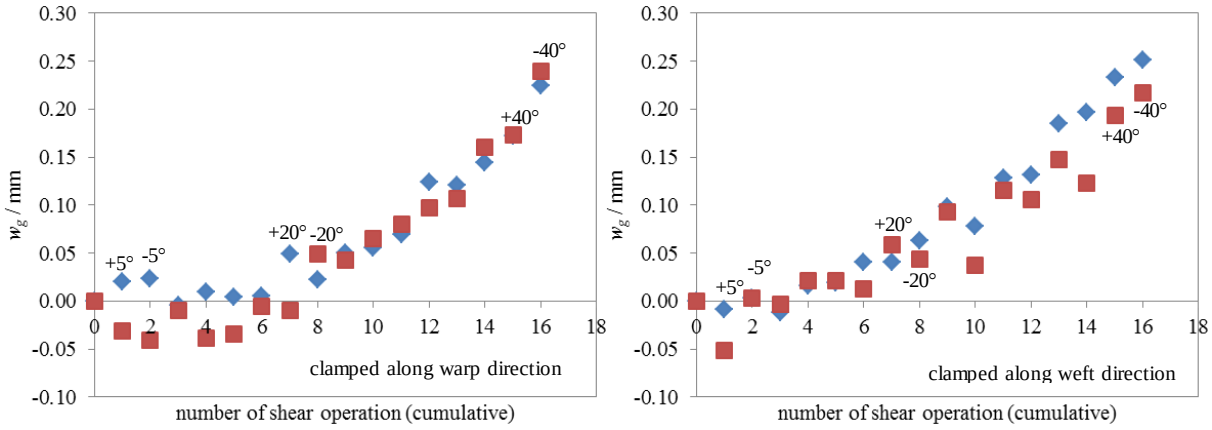

Figure 6. Average width of inter-yarn gaps, w_g, for a specimen of a 2×2 twill weave fabric (S_0 = 660 g/m^2) after undergoing different shear operations; diamond symbols: gap width between warp-yarns; square symbols: gap width between weft-yarns.

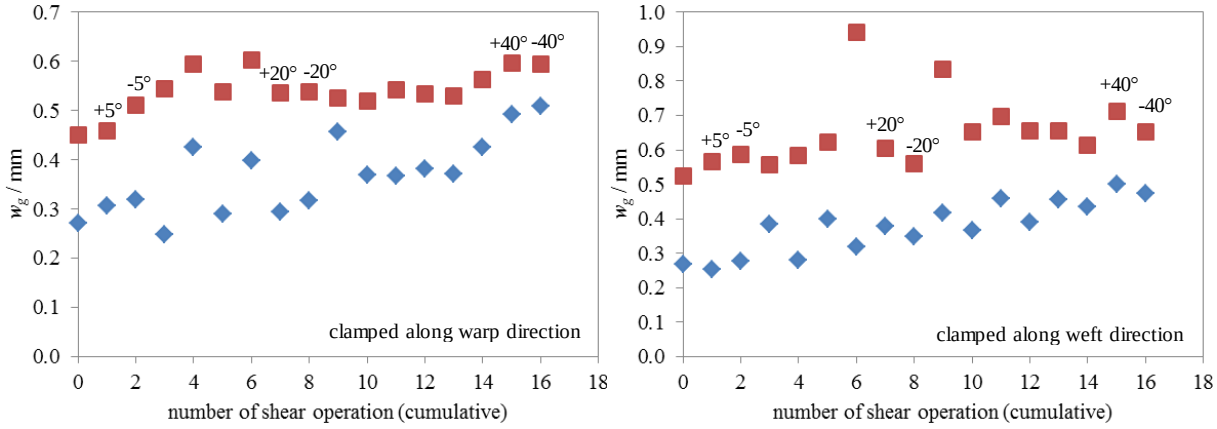

Figure 7. Average width of inter-yarn gaps, w_g, for a specimen of a 2×2 twill weave fabric (S_0 = 285 g/m^2) after undergoing different shear operations; diamond symbols: gap width between warp-yarns; square symbols: gap width between weft-yarns.

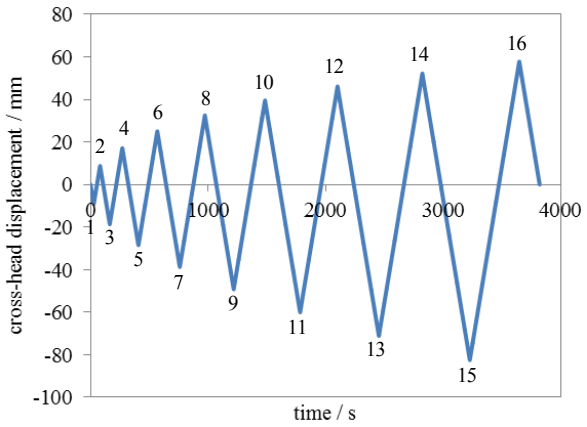

Figure 8. Cross-head displacement as a function of time on testing machine to reproduce shear cycles employed for fabric geometry analysis.

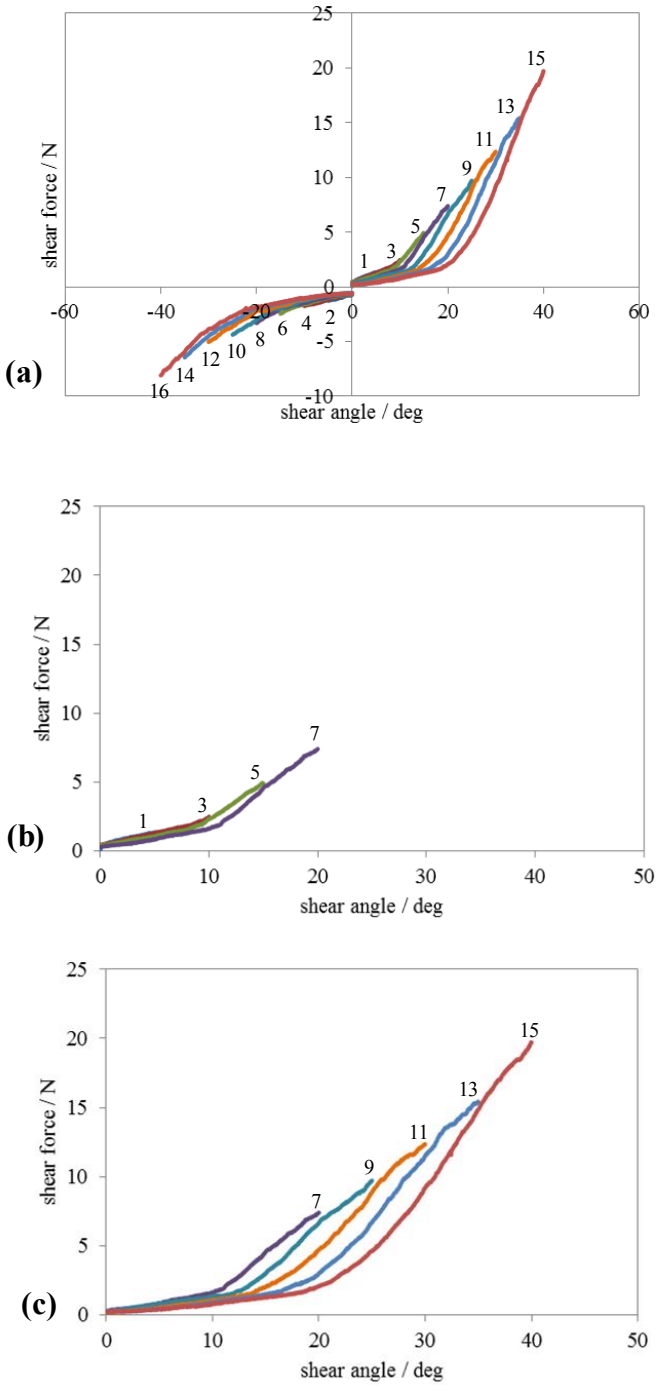

Figure 9. Typical results of picture frame shear tests for the 2×2 twill weave fabric with S_0 = 660 g/m^2, measured for specimens clamped along the fabric warp direction; for clarity, only the loading phase of each shear cycle is plotted; (a): shear force as a function of the shear angle for all shear cycles; (b): top right quadrant, shear cycles 1 to 7; (c): top right quadrant, shear cycles 7 to 15.

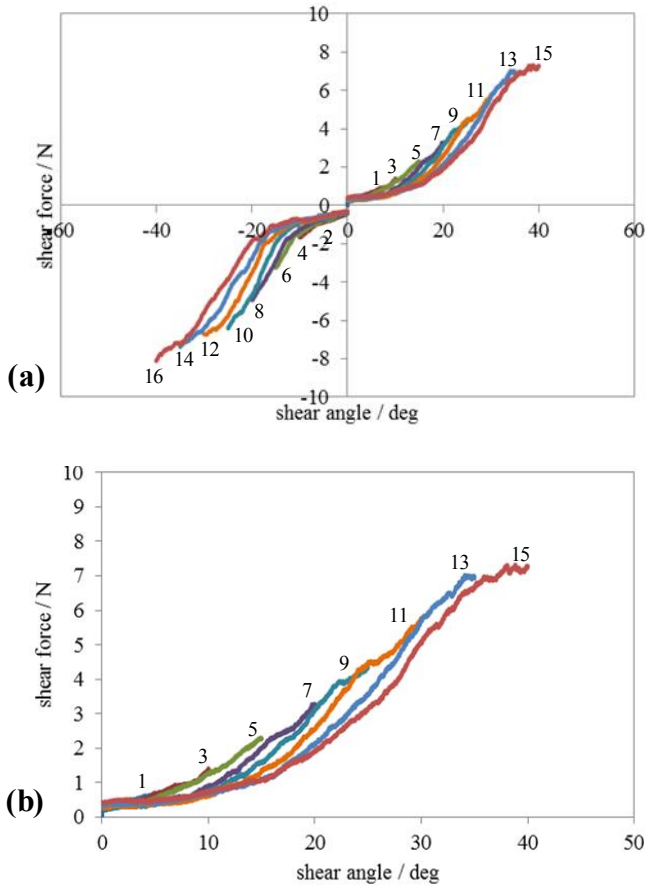

Figure 10. Typical results of picture frame shear tests for the 2×2 twill weave fabric with S_0 = 285 g/m^2, measured for specimens clamped along the fabric warp direction; for clarity, only the loading phase of each shear cycle is plotted; (a): shear force as a function of the shear angle for all shear cycles; (b): top right quadrant, shear cycles 1 to 15.

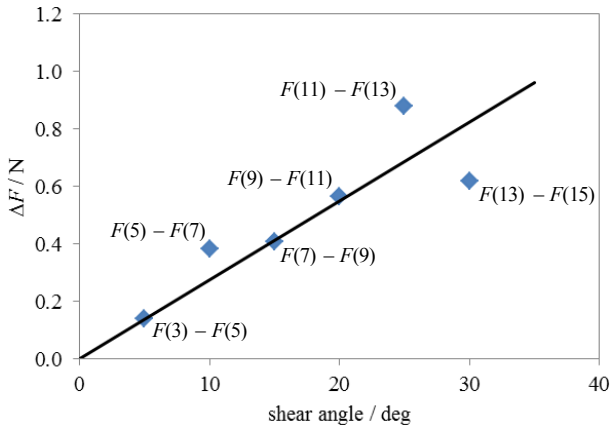

Figure 11. Difference between shear force in subsequent shear cycles, ΔF, measured at different angles (see Figure 10(b)) for the 2×2 twill weave fabric with S_0 = 285 g/m^2.

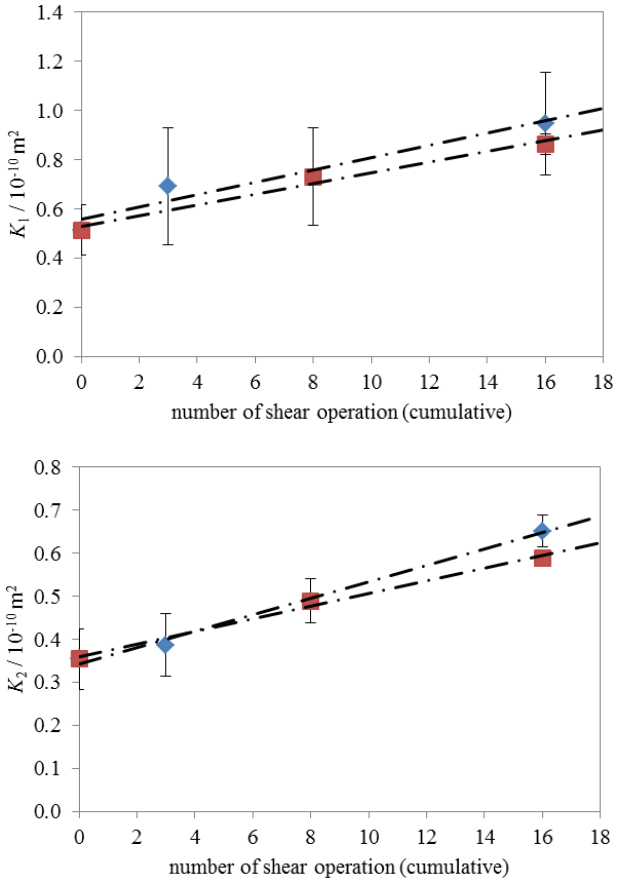

Figure 12. Experimentally determined principal permeability values, K_1 and K_2, for a 2×2 twill weave fabric with S_0 = 660 g/m^2, fibre volume fraction V_f = 0.56, after undergoing different shear operations; diamond symbols: specimens clamped parallel to warp direction during shear; square symbols: specimens clamped parallel to weft direction during shear; error bars indicate standard deviations.

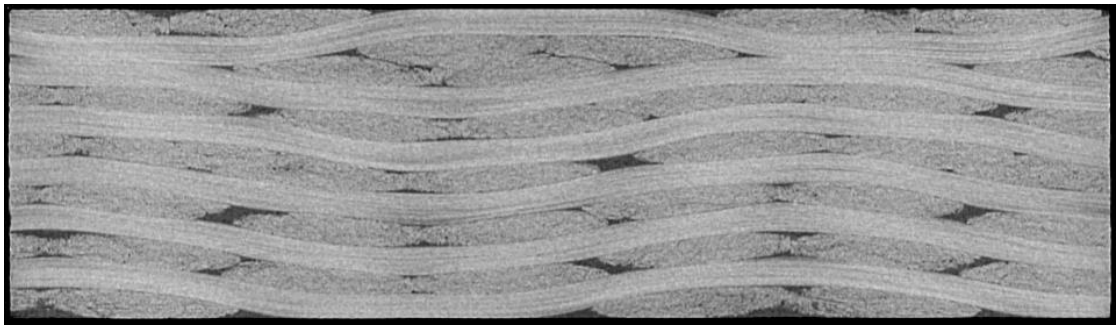

Figure 13. Cross-sectional μ-CT data for 6 layers of the 2×2 twill weave fabric with S_0 = 660 g/m^2 at a specimen thickness of 4 mm (same level of fabric compression as for 3 layers at 2 mm thickness); the fabric was previously unsheared; nesting was random.

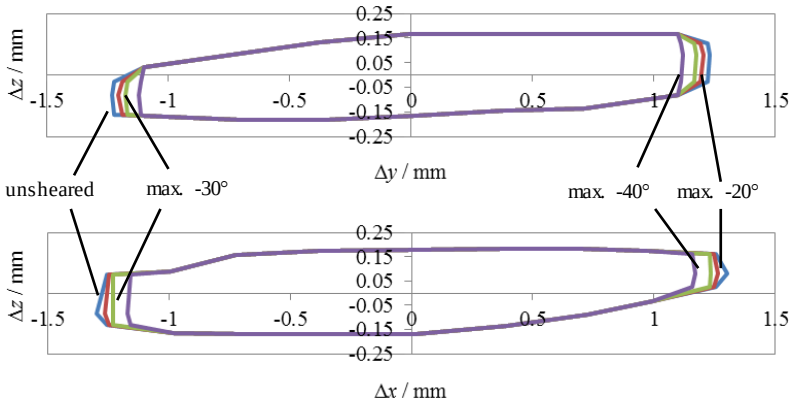

Figure 14. Typical cross-sections of yarns in a 2×2 twill weave fabric with S_0 = 660 g/m^2 in geometrical models for resin flow simulations; Δx, Δy and Δz are co-ordinates relative to the centroid of the cross-sections; top: weft-yarn; bottom: warp-yarn.

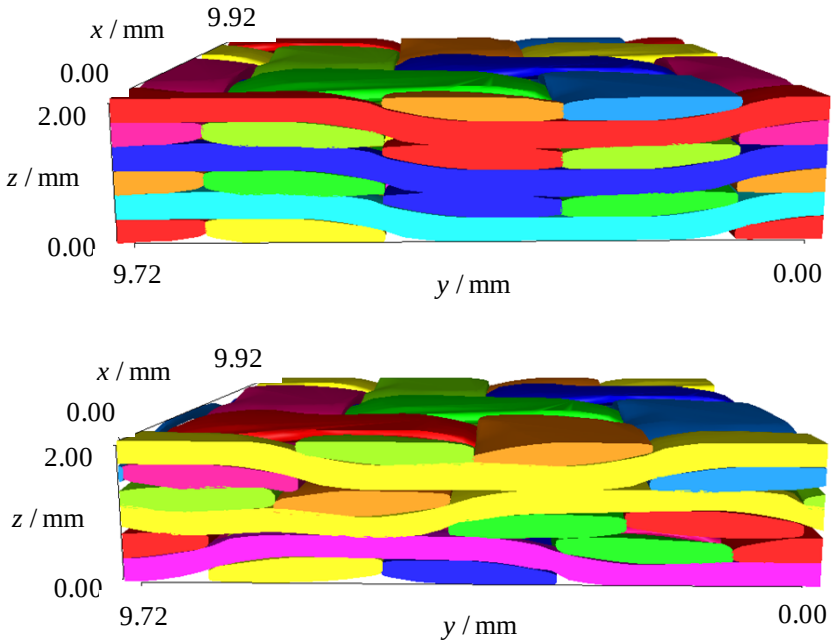

Figure 15. Geometrical models of unsheared lay-up for 2×2 twill weave fabric with S_0 = 660 g/m^2 (3 layers, 2 mm total thickness); top: zero nesting; bottom: random nesting.

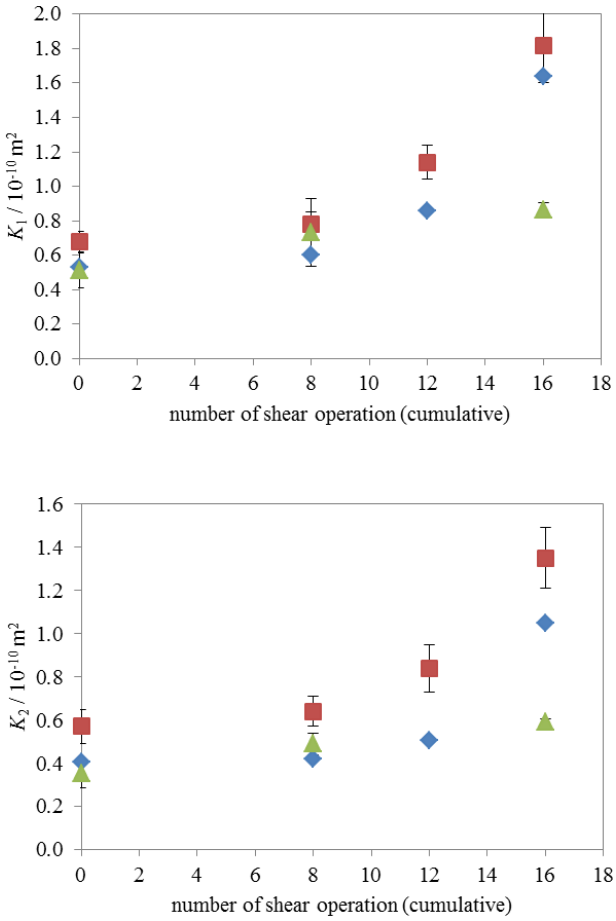

Figure 16. Comparison of measured and predicted permeability values, K_1 and K_2, for a 2×2 twill weave fabric with S_0 = 660 g/m^2, fibre volume fraction V_f = 0.56; diamond symbols: simulation, zero nesting; square symbols: simulation, random nesting; triangular symbols: experiment; error bars indicate standard deviations.

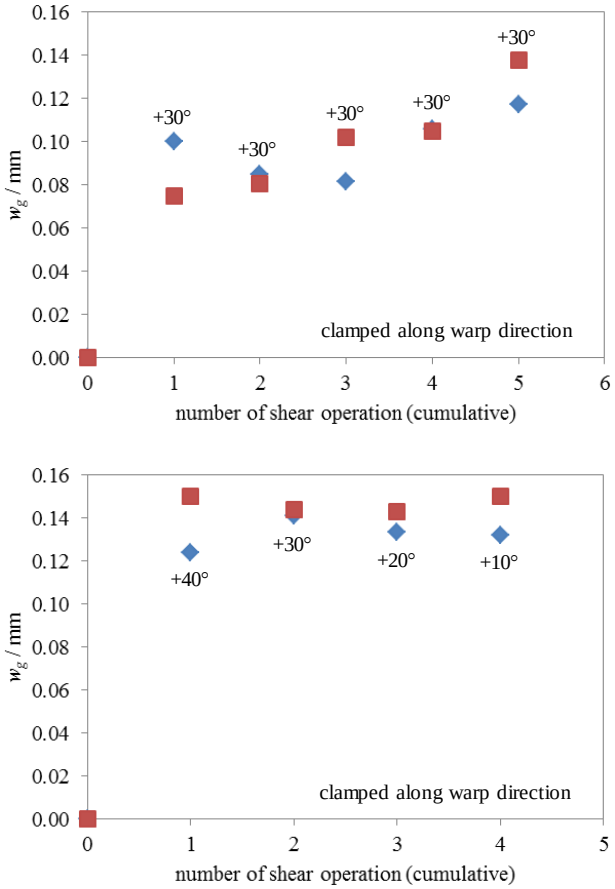

Figure 17. Average width of inter-yarn gaps, w_g, for a specimen of a 2×2 twill weave fabric (S_0 = 660 g/m^2) after undergoing different shear operations; diamond symbols: gap width between warp-yarns; square symbols: gap width between weft-yarns.

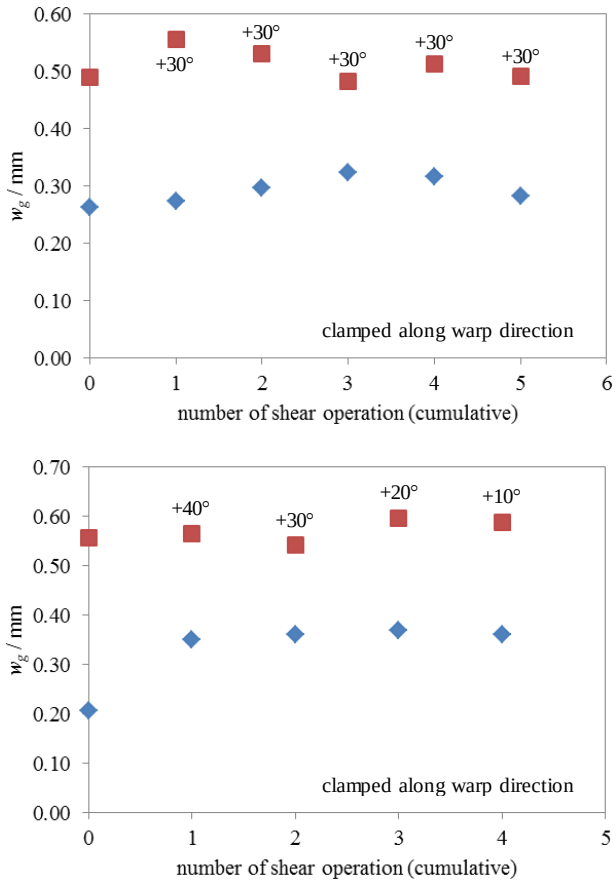

Figure 18. Average width of inter-yarn gaps, w_g, for a specimen of a 2×2 twill weave fabric (S_0 = 285 g/m^2) after undergoing different shear operations; diamond symbols: gap width between warp-yarns; square symbols: gap width between weft-yarns.

Table 1. Width of yarns, w_y, for specimens of two different 2×2 twill weave fabrics, unsheared and after undergoing shear to a maximum angle of -40°, characterised by the superficial densities, S_0; relative changes in average yarn width, $\Delta w_y/w_y$, are also given; average values and standard deviations are given where appropriate.

fabric S_0 / g/m^2	clamped along	w_y / mm (warp) unsheared	w_y / mm (warp) max. -40°	Δw_y / w_y	w_y / mm (weft) unsheared	w_y / mm (weft) max. -40°	Δw_y / w_y
660	warp	2.534 ± 0.079	2.309 ± 0.079	-9 %	2.501 ± 0.065	2.262 ± 0.065	-10 %
	weft	2.595 ± 0.096	2.344 ± 0.076	-10 %	2.459 ± 0.098	2.242 ± 0.115	- 9 %
285	warp	2.640 ± 0.147	2.403 ± 0.173	-9 %	2.412 ± 0.188	2.268 ± 0.255	-6 %
	weft	2.620 ± 0.156	2.415 ± 0.106	-8 %	2.433 ± 0.237	2.306 ± 0.168	-5 %

Table 2. Measured principal permeability values, K_1 and K_2, angle β indicating the orientation of K_1 relative to the fabric weft direction, and ratio, K_1/K_2, for a 2×2 twill weave fabric (S_0 = 660 g/m^2) at a given fibre volume fraction, V_f = 0.56; average values, standard deviations and coefficients of variation (standard deviation / average value) are given where appropriate.

history	K_1 / 10^{-10} m^2	K_2 / 10^{-10} m^2	β	K_1 / K_2
unsheared	0.513 ± 0.102 (± 20 %)	0.354 ± 0.070 (± 20 %)	-39° ± 15°	1.457 ± 0.179 (± 12 %)
sheared, clamped weft, max. -20°	0.732 ± 0.198 (± 27 %)	0.490 ± 0.050 (± 10 %)	-32° ± 30°	1.535 ± 0.596 (± 39 %)
sheared, clamped weft, max. -40°	0.864 ± 0.041 (± 5 %)	0.589 ± 0.016 (± 3 %)	85° ± 29°	1.468 ± 0.098 (± 7 %)
sheared, clamped warp, max. +10°	0.693 ± 0.239 (± 34 %)	0.387 ± 0.073 (± 19 %)	109° ± 23°	1.756 ± 0.362 (± 21 %)
sheared, clamped warp, max. -40°	0.947 ± 0.208 (± 22 %)	0.652 ± 0.038 (± 6 %)	118° ± 17°	1.444 ± 0.234 (± 16 %)

Table 3. Measured principal permeability values, K_1 and K_2, angle β indicating the orientation of K_1 relative to the fabric weft direction, and ratio, K_1/K_2, for a 2×2 twill weave fabric (S_0 = 285 g/m^2) at a given fibre volume fraction, V_f = 0.40; average values, standard deviations and coefficients of variation (standard deviation / average value) are given where appropriate.

history	K_1 / 10^{-10} m^2	K_2 / 10^{-10} m^2	β	K_1 / K_2
unsheared	3.645 ± 0.438 (± 12 %)	2.237 ± 0.248 (± 11 %)	1° ± 14°	1.650 ± 0.289 (± 18 %)

Table 4. Predicted permeability values, K_x and K_y, corresponding to the directions indicated in Figure 15, and ratio K_x/K_y, for specimens of 2×2 twill weave fabric with S_0 = 660 g/m^2 with different shear history and different nesting configuration; fibre volume fraction V_f = 0.56; average values, standard deviations and coefficients of variation (standard deviation / average value) are given where appropriate.

history	nesting	K_y / 10^{-10} m^2	K_x / 10^{-10} m^2	K_x / K_y
unsheared	zero	0.41	0.53	1.31
	random	0.57 ± 0.08 (± 14 %)	0.68 ± 0.06 (± 8 %)	1.22 ± 0.19 (± 15 %)
sheared, clamped weft, max. -20°	zero	0.42	0.60	1.43
	random	0.64 ± 0.07 (± 10 %)	0.78 ± 0.07 (± 9 %)	1.24 ± 0.20 (± 16 %)
sheared, clamped weft, max. -30°	zero	0.50	0.86	1.71
	random	0.84 ± 0.11 (± 13 %)	1.14 ± 0.10 (± 9 %)	1.37 ± 0.22 (± 16 %)
sheared, clamped weft, max. -40°	zero	1.05	1.64	1.56
	random	1.35 ± 0.14 (± 10 %)	1.82 ± 0.22 (± 12 %)	1.37 ± 0.30 (± 22 %)

Table 5. Predicted permeability values, K_{warp} and K_{weft}, and ratio K_{weft}/K_{warp}, for specimens of 2×2 twill weave fabric with $S_0 = 285$ g/m^2 with different shear history and different nesting configuration; fibre volume fraction $V_f = 0.40$; average values, standard deviations and coefficients of variation (standard deviation / average value) are given where appropriate.

history	nesting	K_{warp} / 10^{-10} m^2	K_{weft} / 10^{-10} m^2	K_{weft} / K_{warp}
unsheared	zero	2.20	4.08	1.86
	random	2.50 ± 0.18 (± 7 %)	3.96 ± 0.51 (± 13 %)	1.59 ± 0.22 (± 14 %)
sheared, clamped warp, max. -40°	zero	3.69	5.33	1.44
	random	4.55 ± 0.48 (± 11 %)	5.50 ± 0.50 (± 9 %)	1.22 ± 0.13 (± 11 %)